

ViewMask-1-to-3: Multi-View Consistent Image Generation via Multimodal Diffusion Models

Ruishu Zhu^{1,2*} Zihao Huang^{1,2*} Jiacheng Sun³
Ping Luo⁴ Hongyuan Zhang^{2,4†} Xuelong Li^{2†}

¹School of Artificial Intelligence, OPTics and ElectroNics (iOPEN), Northwestern Polytechnical University

²Institute of Artificial Intelligence of China Telecom (TeleAI)

³Huawei Technologies Co., Ltd.

⁴The University of Hong Kong

{zhuruishu0848, xysunjiacheng, hyzhang98}@gmail.com
huangzhihao@mail.nwpu.edu.cn, pluo@cs.hku.hk, xuelong_li@ieee.org

Abstract

*Motivated by discrete diffusion’s success in language-vision modeling, we explore its potential for multi-view generation, a task dominated by continuous approaches. We introduce **ViewMask-1-to-3**, formulating multi-view synthesis as a discrete sequence modeling problem where each viewpoint is represented as visual tokens from MAGVIT-v2. Through **masked token prediction**, our approach **enables progressive multi-view generation via iterative token unmasking**, unifying language and vision in a shared token space. Importantly, simple random masking combined with self-attention naturally encourages cross-view consistency without specialized architectures or 3D geometric priors. Our method outperforms the baseline on the GSO and 3D-FUTURE benchmarks, ranking first on average across standard image metrics and improving IoU by 10.6% on 3D-FUTURE. This validates discrete diffusion as a promising candidate for multi-view generation.*

1. Introduction

Multi-view image generation has emerged as a fundamental challenge [14, 15, 29], with applications spanning virtual reality [58] and 3D reconstruction [1]. The task aims to generate multiple consistent viewpoints of an object or scene from limited input—typically a single image and accompanying text description. Computational approaches face significant challenges in maintaining geometric consistency, preserving fine-grained details, and ensuring semantic coherence across viewpoints.

Recent advances in this domain have achieved impressive results through diverse technical approaches. **3D representation methods** [30, 42, 46] leverage explicit 3D representations, such as neural radiance fields, 3D Gaussian primitives, or structured latent spaces, to ensure geometric consistency through native 3D modeling and rendering. **Camera-conditioned diffusion models** [19, 22, 28, 39] have demonstrated remarkable flexibility by directly generating multi-view images in 2D space, either controlling the views with precise camera parameters or directly producing a fixed views. **Image Editing model** [18, 27, 31] explore integrating multi-view generation with image editing manner, enabling seamless transitions between different vision tasks. These methods, predominantly built on continuous diffusion in latent space, have collectively established strong baselines.

Meanwhile, a distinct paradigm has shown remarkable success in unified language-vision modeling: discrete diffusion models based on masked token prediction [35, 52, 54]. By operating in a unified vocabulary space, they offer intriguing properties: (1) native multi-modal fusion of text and visual tokens, (2) bidirectional, parallel context modeling during generation, and (3) architectural alignment with large language models. This raises a compelling yet unexplored question: *Can this discrete paradigm serve as a viable alternative for the geometrically demanding task of multi-view generation?*

In this work, we present ViewMask-1-to-3, an exploration of discrete diffusion models for multi-view consistent image generation. Our key insight is to formulate multi-view synthesis as a *discrete sequence modeling problem*, where each viewpoint is represented as a sequence of visual tokens obtained through learned tokenization [55]. By

*Equal Contribution.

†Corresponding Author.

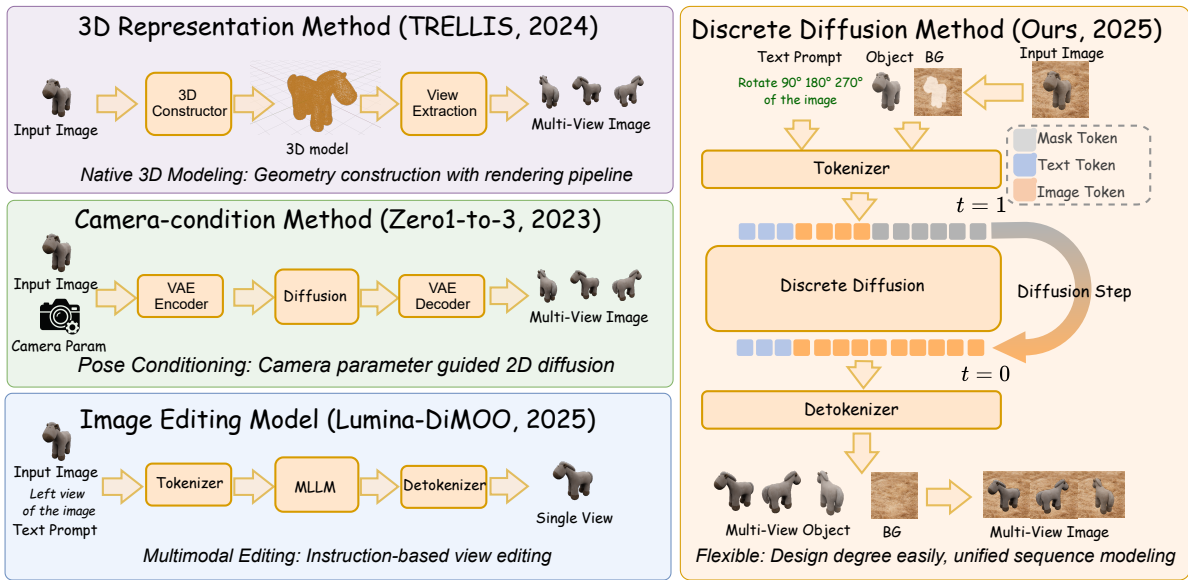


Figure 1. Comparison of multi-view image generation approaches. (Left-Top) 3D representation methods with 3D reconstruction and rendering. (Left-Bottom) Camera-conditioned diffusion methods with precise camera parameters. (Left-middle) Image editing models generate views with sequential manner. (Right) Our discrete diffusion approach enables parallel multi-view generation through unified sequence modeling with flexible text-based control.

extending masked token prediction, a technique proven effective in language modeling [35], to the visual domain with multiple viewpoints, we enable progressive generation through iterative token unmasking. Importantly, we find that a simple random masking strategy, when combined with bidirectional self-attention, naturally encourages cross-view consistency without requiring specialized architectural components or explicit 3D geometric priors. Our contributions are as follows:

- We present a systematic exploration of discrete diffusion models for multi-view image generation, demonstrating that masked token prediction can achieve competitive performance in this domain.
- The proposed simple masking strategy, when combined with bidirectional attention mechanisms, naturally encourages cross-view consistency without requiring 3D geometric priors or specialized architectures.
- We evaluate ViewMask-1-to-3 on standard multi-view generation benchmarks, where it tops the average rankings on image-level metrics (PSNR, SSIM, LPIPS, CD, IOU) for GSO and 3D-FUTURE, particularly achieving a 10.6% higher IoU on 3D-FUTURE.

2. Related Work

2.1. Multi-View Image Generation

3D Representation-Based Methods. Early approaches ensure geometric consistency through explicit 3D modeling. 3D-aware GANs such as π -GAN [4] and EG3D [5] leverage neural radiance fields or tri-plane representations for view-consistent synthesis. More recently, DreamGaussian [42] employs 3D Gaussian Splatting for efficient content creation; TRELIS [46] adopts flow matching to obtain structured 3D latents and then extracts multi-view images; MV-Dream [40] and SyncDreamer [30] integrate NeRF [34] into diffusion frameworks with denoising across viewpoints.

Camera-Conditioned Diffusion Methods. An alternative approach generates multi-view images directly in 2D space through camera-conditioned diffusion. Zero-1-to-3 [28] pioneered fine-tuning pretrained diffusion models with camera pose conditioning for zero-shot novel view synthesis, generating each view independently. Subsequent works address cross-view consistency through various strategies: Zero123++ [39] models the joint distribution of multiple views by concatenating them into a unified representation; SyncDreamer [30] and One-2-3-45 [27] incorporate synchronized denoising and post-processing refinement. Recent extensions include ViVid-1-to-3 [22], which leverages video diffusion for temporal coherence; MV-AR [17],

which introduces autoregressive viewpoint generation; and EpiDiff [19], which enforces epipolar constraints through specialized attention mechanisms. However, these methods typically focus on image-to-multi-view synthesis, with text-to-multi-view requiring additional text-to-image models to generate reference images first.

Image Editing Methods. Recent methods attempt to generate multi-view images via image editing strategies. These approaches leverage various techniques: MV-Adapter [18] transforms text-to-image models into multi-view generators without altering their structure; ImageBrush [53] employs visual instructions rather than text for precise manipulation; SceneScape [10] ensures geometric consistency through depth-aware generation; and Lumina-DiMOO [50] introduces discrete diffusion in image editing with impressive results. While these methods rely on specialized editing strategies, ViewMask-1-to-3 naturally achieves cross-view consistency through token-level modeling using discrete diffusion, offering a more unified and elegant solution to multi-view synthesis.

2.2. Discrete Diffusion Models

D3PM [2] established the foundational framework for discrete diffusion, extending traditional diffusion to discrete state spaces through structured denoising processes. DiffusionBERT [16] demonstrated that pre-trained BERT models could be adapted for text generation through discrete diffusion training. A significant breakthrough came with LLaDA [35], which showed that masked diffusion models can match autoregressive models like LLaMA3-8B in language generation while offering parallel decoding and bidirectional context modeling. LLaDA-V [54] extended this framework to multimodal understanding, demonstrating the potential of discrete diffusion in vision-language tasks. These advances have established discrete diffusion as a viable alternative to autoregressive approaches, for tasks requiring controllable and parallel generation.

2.3. Visual Tokenization

The effectiveness of discrete diffusion for visual tasks critically depends on visual tokenization quality. VQVAE [43] introduced discrete visual representations through vector quantization, laying the groundwork for discrete visual modeling. MaskGIT [6] applied masked token prediction to image generation using vector-quantized representations. MAGVIT-v2 [55] enabling high-quality discrete tokenization for both images and videos through lookup-free quantization and architectural improvements. The success of these tokenizers make discrete approaches increasingly competitive with continuous methods in visual generation tasks.

3. ViewMask-1-to-3

3.1. Overview

Given a single input image $I_0 \in \mathbb{R}^{H \times W \times 3}$ and an optional text description T , our goal is to generate $N = 3$ consistent target views $\{I_1, I_2, I_3\}$ representing the same object from different viewpoints. Beyond image-conditioned view synthesis, our model also achieve text-only generation: provided solely with a description T , it can synthesize $N = 4$ new views $\{I_1, I_2, I_3, I_4\}$ that correspond to distinct viewpoints, even in the absence of an input image. This unified formulation enables both image-to-multi-view and text-to-multi-view generation within a single framework. Unlike Zero-1-to-3 that operates in continuous latent spaces, we formulate multi-view generation as a discrete sequence modeling problem. By representing each view as a sequence of discrete visual tokens, we can **leverage the parallel processing and bidirectional context modeling capabilities of masked diffusion models**.

3.2. Model Design

Our approach consists of three main components: (1) Visual Tokenization, where we convert images to discrete token sequences using MAGVIT-v2; (2) Cross-View Sequence Construction, where we build unified sequences encoding multiple viewpoints with special tokens; and (3) Masked Diffusion Training, where we learn to predict masked visual tokens through iterative refinement.

Visual Tokenization. We adopt MAGVIT-v2 [55] as our visual tokenizer due to its superior performance in discrete visual representation. For an input image I_i , the tokenizer produces a sequence of discrete visual tokens,

$$V^{(i)} = \text{Tokenize}(I_i) = \{v_1^{(i)}, v_2^{(i)}, \dots, v_L^{(i)}\}, \quad (1)$$

where $V^{(i)} \in \mathcal{V}^L$ represents the token sequence, \mathcal{V} is the visual vocabulary with $|\mathcal{V}| = 2^{18}$ tokens, and L is the sequence length. Each token $v_j^{(i)}$ corresponds to a spatial region of the image and encodes local visual features. The discrete representation enables us to apply language modeling techniques directly to visual content while maintaining reconstruction quality through the learned tokenizer.

The tokenized sequences are then embedded into the language model’s embedding space:

$$\mathbf{e}^{(i)} = \text{Embed}(V^{(i)}) \in \mathbb{R}^{L \times d}, \quad (2)$$

where d is the embedding dimension of the transformer.

Cross-View Sequence Construction. The unified sequence construction is a core step of ViewMask-1-to-3, which enables coordinated generation across multiple viewpoints under both image-to-multi-view (I2MV) and text-to-multi-view (T2MV) settings. By using the same masked-sequence format, we minimize the structural gap between

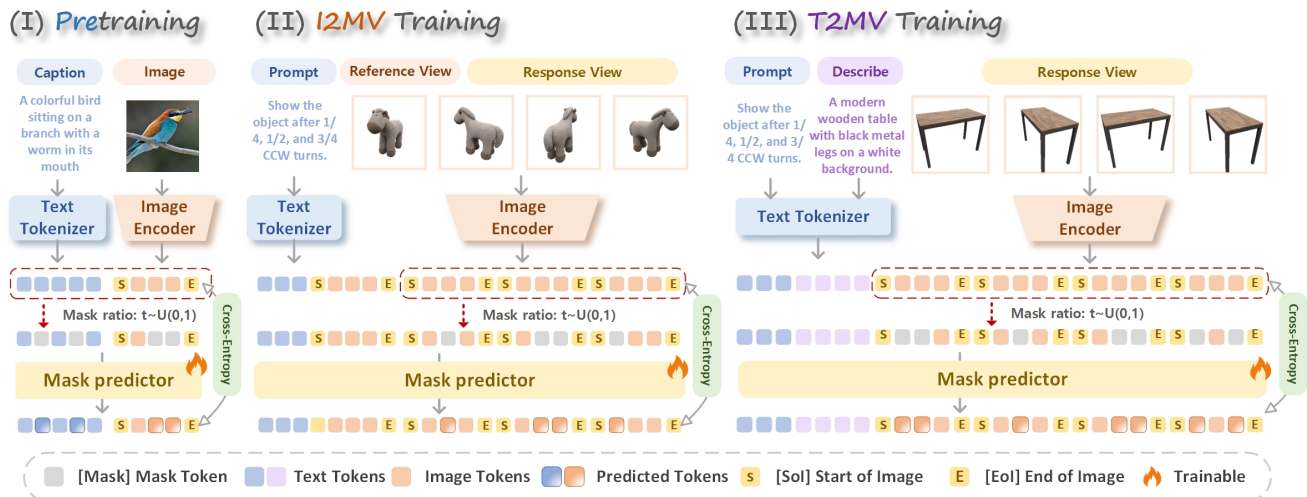


Figure 2. **Overview of our three-stage training framework.** (I) **Stage 1:** Pretraining aligns text and image modalities using masked image-caption sequences. (II) **Stage 2:** Image-to-Multi-View (I2MV) masks the target view and learns to reconstruct it conditioned on a reference view, thereby acquiring multi-view generation capability. (III) **Stage 3:** Text-to-Multi-View (T2MV) masks all views and learns to generate multiple views of an object conditioned on a text description.

I2MV and T2MV inputs, enabling the model to treat both tasks similarly (see Section 3.3 for details).

Cross-View Masking Strategy. During training, we employ a simple yet effective random masking strategy. For each training sample, target tokens are first selected based on the current training stage (see Section 3.3), and a masking ratio $r \sim \text{Uniform}(0, 1)$ is sampled to randomly replace a subset of them with a special [MASK] token.

3.3. Multi-Stage Training Strategy

As shown in Fig. 2, our training framework comprises three stages.

Stage1: Pretraining for Multimodal Alignment. To enable the LLADA model to learn representations of image tokens, we leverage image-caption pairs to align the two modalities. The input sequence is formatted as:

[T2I] [SOT] *caption tokens* [EOT] [SOI] *image tokens* [EOI],

where [T2I] indicates the image-caption alignment, [SOT] and [EOT] denote the start and end of the text, and [SOI] and [EOI] denote the start and end of the image. Both *caption tokens* and *image tokens* are randomly masked with a certain probability during training. This design encourages the model to fully capture the co-occurring semantic information in image-caption pairs, thereby aligning the representations of the two modalities.

We construct a multimodal pretraining corpus of 1.2 million image-caption pairs using the images from ImageNet [9] images combined with captions provided by

imagenet-1k-vl-enriched [24], to facilitate alignment between modalities.

Stage2: Image to Multi-View. To enable the LLADA model to learn representations of image tokens, we leverage image-caption pairs to align the two modalities. The input sequence is formatted as:

[I2MV] [SOT] P . [EOT] [SOI] R . [EOI] [SOI] $G_1 G_2 G_3$ [EOI],

where [I2MV] indicates the image-to-multi-view task, P represents the prompt tokens, R represents the reference image tokens, and G_i represents the generated image tokens. For brevity, the repeated [EOI] [SOI] between consecutive G_i are omitted. G_i are randomly masked with a certain probability during training.

At this stage, the model is trained on a curated subset of Objaverse [8] and Habitat Synthetic Scene Dataset (HSSD) [21]. Following the data split provided by Objaverse++ [25], we removed samples labeled as Low Quality (No semantic meaning. Objects that annotators cannot identify or are corrupted), to ensure more stable training.

Stage3: Text to Multi-View. To extend the I2MV paradigm to T2MV, we incorporate an additional textual description specifying the target views immediately after the prompt. Accordingly, the input sequence is formatted as:

[T2MV] [SOT] P . D . [EOT] [SOI] $G_1 G_2 G_3 G_4$ [EOI],

where [T2MV] indicates the text-to-multi-view task, D represents the description tokens. For brevity, the repeated [EOI] [SOI] between consecutive G_i are omitted. G_i are randomly masked with a certain probability during training.

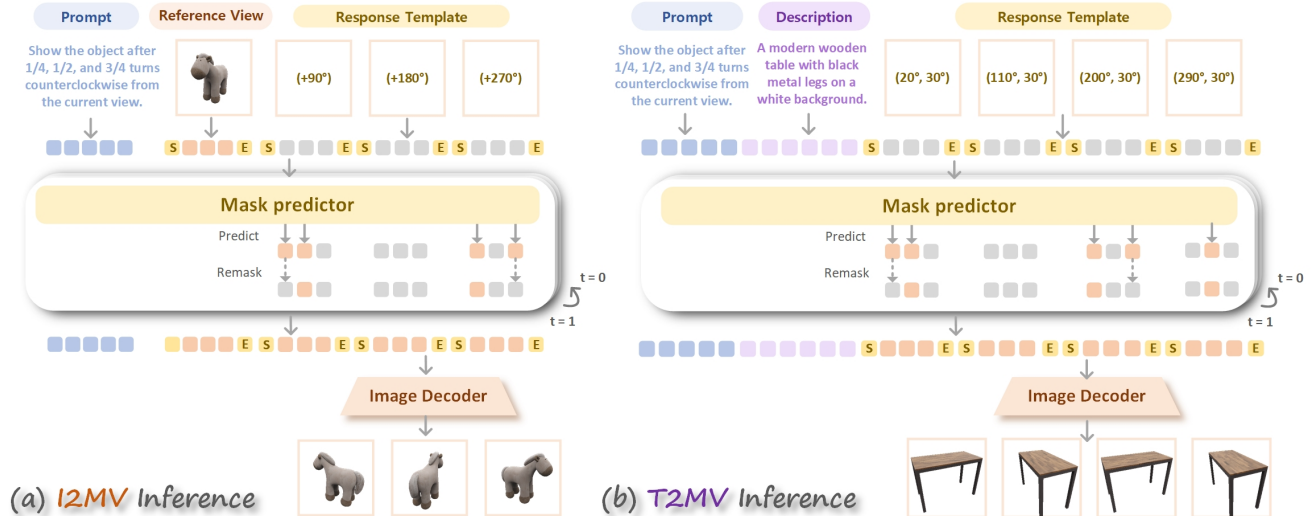


Figure 3. **Overview of inference framework.** (a) **I2MV**: The tokenized prompt and reference view provide a template for generating three consistent output images from different viewpoints. (b) **T2MV**: Tokenized prompt and description, providing a template for generating four output images. At each timestep t , the tokens are further predicted, and under the guidance of the mask schedule, re-masking is performed based on confidence.

We enhance Objaverse with Cap3D [32, 33], which offers detailed textual descriptions for 3D assets.

Loss. ViewMask-1-to-3 is trained using a cross-entropy loss that predicts original tokens at masked positions.

$$\mathcal{L}_{\text{CE}} = - \sum_{i=1}^3 \sum_{j \in \mathcal{M}_i} \log P(v_j^{(i)} | s_{\setminus \mathcal{M}}), \quad (3)$$

where \mathcal{M}_i denotes the set of masked positions in view i , and $s_{\setminus \mathcal{M}}$ represents the sequence with masked tokens. This objective encourages the model to reconstruct original visual tokens while leveraging unmasked context from the input image, text description, and partially observed target views. The cross-attention mechanism naturally enables information flow between different modalities and viewpoints.

3.4. Inference Process

Construction of Input Sequences. During inference, we perform iterative denoising starting from fully masked target views, as illustrated in Fig. 3. For **I2MV**, the model is provided with a tokenized prompt and the reference view. The template is designed to generate three output images. For **T2MV**, the input consists of a tokenized prompt and a textual description of the desired view. This template supports the generation of four output images.

Predict and Remask. We employ an iterative denoising-based sampling strategy. The model progressively predicts token distributions over T iterations. At each step, the model performs a forward pass to obtain logits for all

masked positions and estimates the confidence of each token prediction. A scheduling function (cosine, linear, or quadratic) determines the number of tokens to be re-masked in the next step, where low-confidence tokens are re-masked while high-confidence ones are retained. This *predict–re-mask* loop continues until all masked tokens are generated, progressively refining the sequence toward the final output. We further discuss the effects of different scheduling strategies in the ablation study (see Section 4.3).

4. Experiments

Datasets. Our model was trained on a subset of Objaverse [8] and HSSD [21]. Following the data split provided by Objaverse++ [25], we removed samples labeled as Low Quality, to ensure more stable training. To enrich the textual supervision, we adopted the Cap3D [32, 33] annotations, which provide descriptive captions for 3D objects. In total, we used 180K 3D objects, each rendered as an 8-frame RGBA orbit sequence at a resolution of 256×256, with the elevation fixed at 30°. During training, one frame was randomly selected as the reference image for each object, resulting in a multi-view generation dataset.

Metrics. We evaluate the multi-view generation results from two perspectives. First, for the directly generated novel views, we adopt common image-level metrics, including Peak Signal-to-Noise Ratio (PSNR), Structural Similarity Index Measure (SSIM) [44], and Learned Perceptual Image Patch Similarity (LPIPS) [56], to assess visual fidelity and perceptual quality. Then, we employ InstantMesh [51]

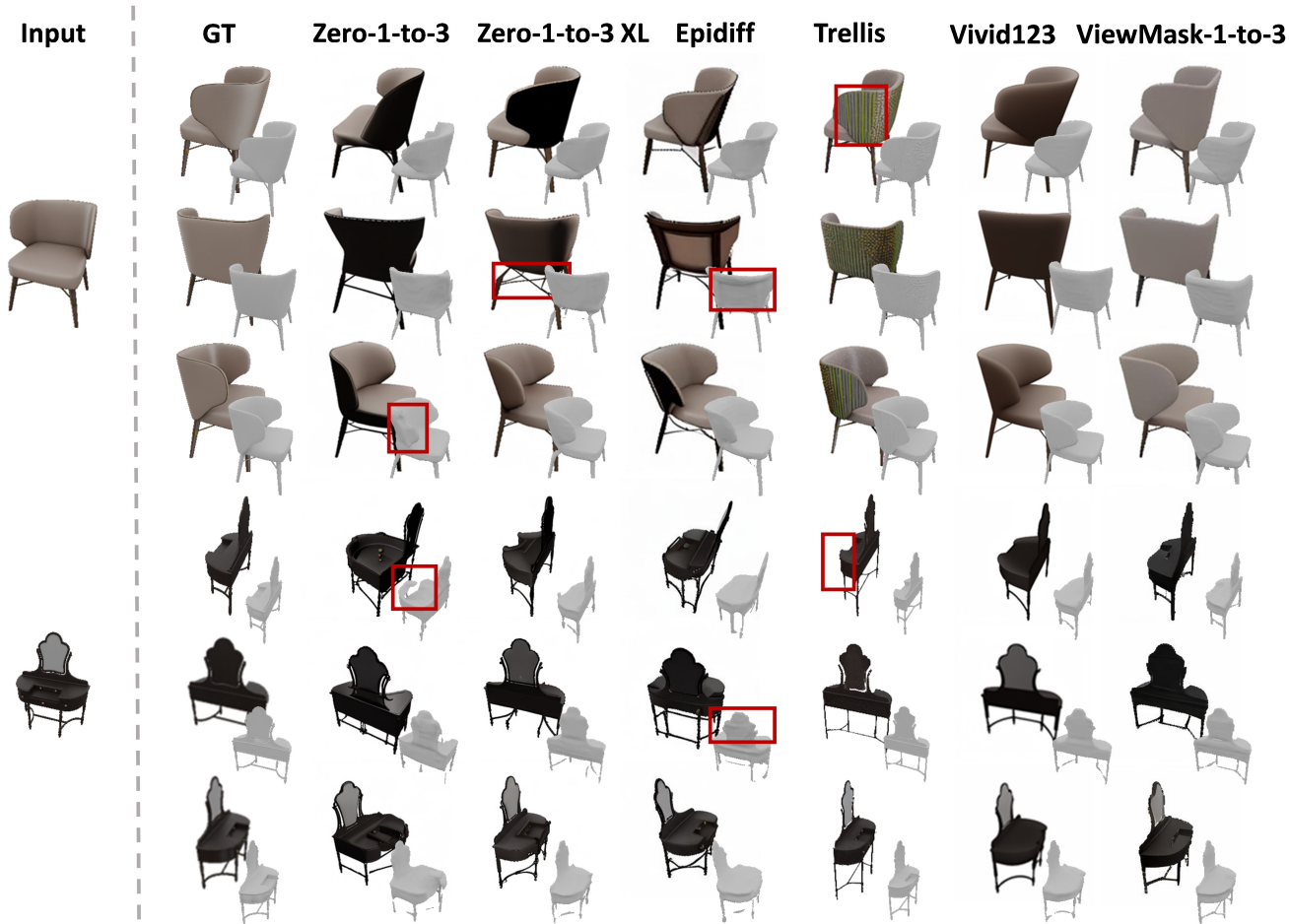


Figure 4. **Qualitative comparison on the 3D-Future dataset.** Visual results on the 3D-Future dataset, where the bottom-right shows the reconstructed mesh, demonstrating that our ViewMask-1-to-3 produces more consistent and realistic novel views compared with recent methods.

to reconstruct 3D geometry from the generated views, and evaluate the resulting point clouds using Chamfer Distance (CD) and Intersection over Union (IoU) to quantify geometric consistency and accuracy.

4.1. Image to Multi-view Images

Baseline. We compare our method against a comprehensive set of state-of-the-art diffusion-based novel view generation approaches, including Zero-1-to-3 [28], Zero-1-to-3 XL [7, 28], ViVid-1-to-3 [22], Zero123++ [39], MV-Adapter [18], EpiDiff [19], AR-1-to-3 [57], and TRELLIS [46].

Qualitative Results.

Fig. 4 presents a visual comparison between our method and several state-of-the-art multi-view generation approaches. In the top three rows, ViewMask-1-to-3 preserves accurate chair legs and seat curvature, avoiding the distortions and artifacts seen in other methods. In the bot-

tom three rows, it achieves the best overall consistency, capturing both the recessed details on the desktop and the metal frame. Compared with these baselines, our method produces sharper visual quality, better preserves fine-grained textures, and maintains higher cross-view consistency.

Quantitative Results. To quantitatively evaluate the zero-shot generalization capability of our model, we conduct experiments on two aspects: (1) *image-level quality*, measured on novel views generated from a single input image, and (2) *3D-level geometric accuracy*, evaluated on 3D reconstructions. These experiments are evaluated on the Google Scanned Objects (GSO) dataset [50] and the 3D-FUTURE dataset [11].

The input views are selected with controlled offsets in azimuth and elevation relative to the canonical frontal view of each 3D object. For models that support arbitrary-angle rendering, such as Zero-1-to-3 and Zero-1-to-3 XL, the

Table 1. **Quantitative comparison on multi-view generation over the GSO and 3D-FUTURE datasets.** We report PSNR, SSIM, and LPIPS.

Method	Architecture	GSO			3D-FUTURE			Rank
		PSNR \uparrow	SSIM \uparrow	LPIPS \downarrow	PSNR \uparrow	SSIM \uparrow	LPIPS \downarrow	
Zero-1-to-3 [28]	2D Cont. Diff.	18.8219	0.8294	0.1659	17.0526	0.8163	0.1760	5.3
Zero-1-to-3 XL [28]	2D Cont. Diff.	19.6839	0.8381	<u>0.1518</u>	18.4702	0.8337	<u>0.1485</u>	<u>3.0</u>
ViVid-1-to-3 [22]	2D Cont. Diff.	<u>19.7978</u>	0.8566	0.1764	18.3241	0.8437	0.1682	3.5
Zero123++ [39]	2D Cont. Diff.	19.6373	0.8045	0.3550	23.5001	<u>0.8527</u>	0.1529	4.3
Epidiff [19]	2D Cont. Diff.	18.9917	0.8244	0.1667	17.4592	0.8108	0.1785	5.7
MV-Adapter [18]	2D Cont. Diff.	19.4673	0.7518	0.1503	19.3375	0.7217	0.4036	5.8
AR-1-to-3 [57]	Video Cont. Diff.	13.5084	0.7376	0.3514	13.7724	0.7479	0.3034	8.5
TRELLIS [46]	3D Rectified Flow	14.4493	0.8058	0.3223	14.4604	0.7896	0.2990	7.2
ViewMask-1-to-3	2D Disc. Diff.	20.3868	0.8549	0.1537	19.8186	0.8610	0.1315	1.7

Table 2. **Quantitative comparison on 3D reconstruction over the GSO and 3D-FUTURE datasets.** We report chamfer distance (CD) value and IOU. \uparrow indicates higher is better, \downarrow indicates lower is better.

Method	GSO		3D-FUTURE	
	CD \downarrow	IOU \uparrow	CD \downarrow	IOU \uparrow
Zero-1-to-3	0.0163	0.5665	0.0113	0.5005
Zero-1-to-3 XL	<u>0.0159</u>	0.5799	<u>0.0106</u>	<u>0.5271</u>
Zero123++	0.0163	0.5832	0.0314	0.4250
ViVid-1-to-3	0.0163	<u>0.5841</u>	0.0105	0.5246
AR-1-to-3	0.0372	0.4380	0.0148	0.4286
EpiDiff	0.0166	0.5457	0.0121	0.4784
TRELLIS	0.0496	0.4026	0.0178	0.4396
ViewMask-1-to-3	0.0149	0.5847	<u>0.0106</u>	0.5315

views are rendered at the same angles as those used by ViewMask-1-to-3 to ensure a fair comparison. We then evaluate PSNR, SSIM, and LPIPS following each model’s respective settings, and report the results in Tab. 1. Overall, our method, ViewMask-1-to-3, achieves the best combined performance across both datasets and attains the highest rank (1.7), demonstrating its superiority in multi-view generation.

To evaluate geometric consistency, we reconstruct 3D shapes from the generated multi-view images for each model. We then compute Chamfer Distance (CD) and IoU between the reconstructed shapes and the ground-truth meshes. The quantitative results are reported in Tab. 2, demonstrating that our method achieves lower CD and higher IoU, indicating more accurate 3D reconstruction and better cross-view consistency.

4.2. Text to Multi-view Images

In the T2MV task, we demonstrate the ability to generate multi-view images of an object directly from text inputs. Models like MV-Adapter [18] and TRELLIS [46] support T2MV and I2MV using different checkpoints or

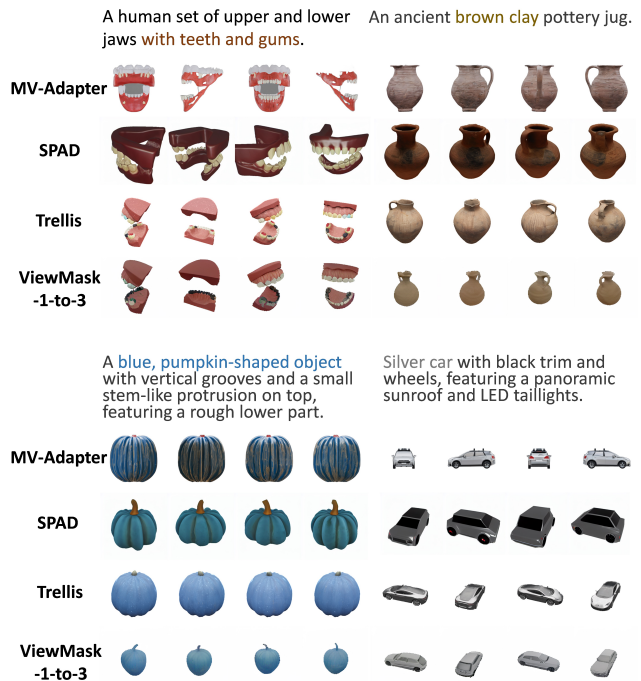


Figure 5. **Qualitative results on T2MV.** Examples of multi-view object generation from text prompts using our method, achieved directly without any intermediate steps.

architectures. Zero123++ [39] and ViVid-1-to-3 [22] generate reference images with a T2I model before extracting the subject for novel views. In contrast, our method directly produces novel views that preserve both the specified viewpoint and the prompt’s semantic content. As shown in Fig. 5, we present representative test samples from the Objaverse dataset and compare qualitative results with MV-Adapter [18], TRELLIS [46], and SPAD [20], showing that our method achieves comparable visual quality and consistency.

4.3. Ablation study

Mask Schedule. We investigate the impact of different mask scheduling strategies on our model’s performance, including linear, quadratic, and cosine schedules.

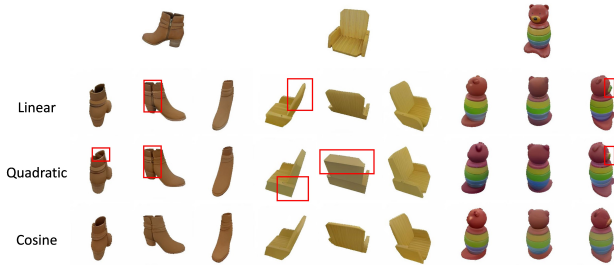


Figure 6. **Qualitative results of different mask scheduling strategies on a subset of the GSO dataset.** Compared with linear, quadratic, and fixed schedules, the cosine schedule produces sharper details and more coherent structures in the generated novel views.

In Tab. 3, our experiments on a subset of the GSO dataset indicate that the cosine schedule yields smoother optimization and superior final results compared with the other strategies, highlighting the importance of gradually adjusting the masking ratio over timesteps. In addition to quantitative evaluation, we provide qualitative visualizations of the generated images under different schedules, as shown in Fig. 6. For the boot, both the linear and quadratic schedules hallucinate an additional zipper on the opposite side, which is clearly inconsistent with reality. For the chair, the quadratic schedule yields incorrect thickness estimation. For the toy, both the linear and quadratic schedules distort the teddy bear’s facial region.

Table 3. **Ablation study on different mask scheduling strategies.** The metrics (e.g., PSNR, SSIM, LPIPS) are reported for each schedule.

Schedule	PSNR \uparrow	SSIM \uparrow	LPIPS \downarrow
Linear	17.9882	0.8435	0.1882
Quadratic	17.9785	0.8431	0.1865
Cosine	18.0974	0.8437	0.1834

4.4. Task Extension

Unified Multimodal Understanding and Generation. In addition to the aforementioned I2MV and T2MV capabilities, the Stage-1 pretraining endows our model with fundamental multimodal understanding and text-to-image generation abilities. As shown in Fig. 7, the model can perform basic understanding and generation tasks without any additional fine-tuning. Building on these abilities, our model

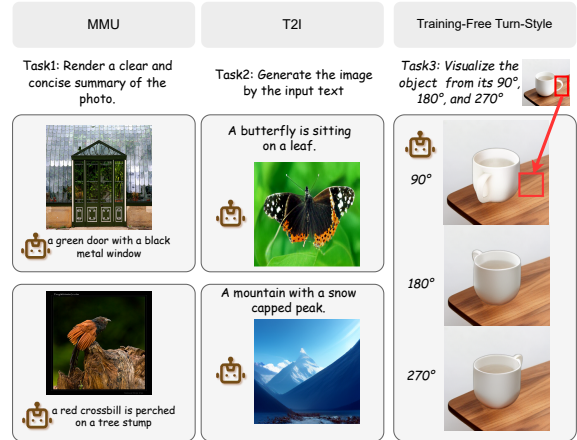


Figure 7. **Task Extension.** Left: basic multimodal understanding (MMU), e.g., captioning. Middle: text-to-image (T2I) generation without fine-tuning. Right: training-free 2D turn-style and completion preserving the background.

naturally extends toward unified multimodal understanding and generation, evaluated on GenEval [13] for compositional text-to-image generation. ViewMask-1-to-3 achieves the best overall score (0.72), outperforming unified models Show-o (0.68) [49] and MMaDA (0.63) [52], and surpassing generation-only models like DALL-E 3 (0.67) [3], comparable to SANA-1.5 (0.72) [48], as shown in Table 4. Compared with the architecturally similar MMaDA, ViewMask-1-to-3 achieves a 14% overall improvement (0.72 vs. 0.63). This significant gain highlights the practical potential of discrete diffusion architectures.

Training-Free 2D Turn-Style. Inspired by Adobe’s Project Turn Style, which enables re-angling and rotating 2D illustrations as if they were 3D objects, we extend this capability in a *training-free* manner based on our ViewMask-1-to-3 framework. Benefiting from the inherent properties of discrete diffusion, our model can rotate a specified object by a given angle and perform image completion while preserving the original background, all without additional fine-tuning, as these abilities are implicitly embedded during diffusion training. These cases show that our framework extends to a unified diffusion architecture while maintaining strong flexibility and generalization across diverse tasks.

5. Conclusion

In this work, we introduce **ViewMask-1-to-3**, a discrete diffusion framework for multi-view image generation. Experiments on GSO and 3D-FUTURE demonstrate its strong performance, showcasing discrete diffusion as an effective and flexible approach for multi-view synthesis. Our results also highlight its potential for MMU, T2I, T2MV, and

training-free 2D turn-style, paving the way toward more unified and scalable multi-view generation.

Despite strong performance, there is room to expand viewpoint diversity and improve lighting robustness. Future work will focus on enhancing scalability, resolution, and generalization for more unified multi-view generation.

Acknowledgements

This paper is partially supported by the National Key R&D Program of China No.2022ZD0161000.

References

- [1] Hadi Alzayer, Kevin Zhang, Brandon Feng, Christopher A Metzler, and Jia-Bin Huang. Seeing the world through your eyes. In *Proceedings of the IEEE/CVF Conference on Computer Vision and Pattern Recognition*, pages 4864–4873, 2024. 1
- [2] Jacob Austin, Daniel D Johnson, Jonathan Ho, Daniel Tarlow, and Rianne Van Den Berg. Structured denoising diffusion models in discrete state-spaces. *Advances in neural information processing systems*, 34:17981–17993, 2021. 3
- [3] James Betker, Gabriel Goh, Li Jing, Tim Brooks, Jianfeng Wang, Linjie Li, Long Ouyang, Juntang Zhuang, Joyce Lee, Yufei Guo, et al. Improving image generation with better captions. *Computer Science*. <https://cdn.openai.com/papers/dall-e-3.pdf>, 2(3):8, 2023. 8, 1
- [4] Eric R Chan, Marco Monteiro, Petr Kellnhofer, Jiajun Wu, and Gordon Wetzstein. pi-gan: Periodic implicit generative adversarial networks for 3d-aware image synthesis. In *Proceedings of the IEEE/CVF conference on computer vision and pattern recognition*, pages 5799–5809, 2021. 2
- [5] Eric R Chan, Connor Z Lin, Matthew A Chan, Koki Nagano, Boxiao Pan, Shalini De Mello, Orazio Gallo, Leonidas J Guibas, Jonathan Tremblay, Sameh Khamis, et al. Efficient geometry-aware 3d generative adversarial networks. In *Proceedings of the IEEE/CVF conference on computer vision and pattern recognition*, pages 16123–16133, 2022. 2
- [6] Huiwen Chang, Han Zhang, Lu Jiang, Ce Liu, and William T. Freeman. Maskgit: Masked generative image transformer. In *Proceedings of the IEEE/CVF Conference on Computer Vision and Pattern Recognition (CVPR)*, pages 11315–11325, 2022. 3
- [7] Matt Deitke, Ruoshi Liu, Matthew Wallingford, Huong Ngo, Oscar Michel, Aditya Kusupati, Alan Fan, Christian Laforte, Vikram Voleti, Samir Yitzhak Gadre, Eli VanderBilt, Aniruddha Kembhavi, Carl Vondrick, Georgia Gkioxari, Kiana Ehsani, Ludwig Schmidt, and Ali Farhadi. Objaverse-xl: A universe of 10m+ 3d objects. *arXiv preprint arXiv:2307.05663*, 2023. 6, 1
- [8] Matt Deitke, Dustin Schwenk, Jordi Salvador, Luca Weihs, Oscar Michel, Eli VanderBilt, Ludwig Schmidt, Kiana Ehsani, Aniruddha Kembhavi, and Ali Farhadi. Objaverse: A universe of annotated 3d objects. In *Proceedings of the IEEE/CVF conference on computer vision and pattern recognition*, pages 13142–13153, 2023. 4, 5
- [9] Jia Deng, Wei Dong, Richard Socher, Li-Jia Li, Kai Li, and Li Fei-Fei. Imagenet: A large-scale hierarchical image database. In *2009 IEEE conference on computer vision and pattern recognition*, pages 248–255. Ieee, 2009. 4
- [10] Rafail Fridman, Amit Abecasis, Yoni Kasten, and Tali Dekel. Scenescape: Text-driven consistent scene generation. *Advances in Neural Information Processing Systems*, 36:39897–39914, 2023. 3
- [11] Huan Fu, Rongfei Jia, Lin Gao, Mingming Gong, Binqiang Zhao, Steve Maybank, and Dacheng Tao. 3d-future: 3d furniture shape with texture, 2020. 6
- [12] Yuying Ge, Sijie Zhao, Jinguo Zhu, Yixiao Ge, Kun Yi, Lin Song, Chen Li, Xiaohan Ding, and Ying Shan. Seed-x: Multimodal models with unified multi-granularity comprehension and generation. *arXiv preprint arXiv:2404.14396*, 2024. 1
- [13] Dhruva Ghosh, Hanna Hajishirzi, and Ludwig Schmidt. Geneval: An object-focused framework for evaluating text-to-image alignment, 2023. 8
- [14] Qianyun He, Xinya Ji, Yicheng Gong, Yuanxun Lu, Zhengyu Diao, Linjia Huang, Yao Yao, Siyu Zhu, Zhan Ma, Songcen Xu, et al. Emotalk3d: High-fidelity free-view synthesis of emotional 3d talking head. In *European Conference on Computer Vision*, pages 55–72. Springer, 2024. 1
- [15] Yuxiao He, Yiyu Zhuang, Yanwen Wang, Yao Yao, Siyu Zhu, Xiaoyu Li, Qi Zhang, Xun Cao, and Hao Zhu. Head360: Learning a parametric 3d full-head for free-view synthesis in 360 degree. In *European Conference on Computer Vision*, pages 254–272. Springer, 2024. 1
- [16] Zhengfu He, Tianxiang Sun, Qiong Tang, Kuanning Wang, Xuan-Jing Huang, and Xipeng Qiu. Diffusionbert: Improving generative masked language models with diffusion models. In *Proceedings of the 61st Annual Meeting of the Association for Computational Linguistics (Volume 1: Long Papers)*, pages 4521–4534, 2023. 3
- [17] JiaKui Hu, Yuxiao Yang, Jialun Liu, Jinbo Wu, Chen Zhao, and Yanye Lu. Auto-regressively generating multi-view consistent images. *arXiv preprint arXiv:2506.18527*, 2025. 2
- [18] Zehuan Huang, Yuanchen Guo, Haoran Wang, Ran Yi, Lizhuang Ma, Yan-Pei Cao, and Lu Sheng. Mv-adapter: Multi-view consistent image generation made easy. *arXiv preprint arXiv:2412.03632*, 2024. 1, 3, 6, 7
- [19] Zehuan Huang, Hao Wen, Junting Dong, Yaohui Wang, Yanguang Li, Xinyuan Chen, Yan-Pei Cao, Ding Liang, Yu Qiao, Bo Dai, and Lu Sheng. Epidiff: Enhancing multi-view synthesis via localized epipolar-constrained diffusion, 2024. 1, 3, 6, 7
- [20] Yash Kant, Ziyi Wu, Michael Vasilkovsky, Guocheng Qian, Jian Ren, Riza Alp Guler, Bernard Ghanem, Sergey Tulyakov, Igor Gilitschenski, and Aliaksandr Siarohin. Spad : Spatially aware multiview diffusers, 2024. 7
- [21] Mukul Khanna*, Yongsan Mao*, Hanxiao Jiang, Sanjay Haresh, Brennan Shacklett, Dhruv Batra, Alexander Clegg, Eric Undersander, Angel X. Chang, and Manolis Savva. Habitat Synthetic Scenes Dataset (HSSD-200): An Analysis of 3D Scene Scale and Realism Tradeoffs for ObjectGoal Navigation. *arXiv preprint*, 2023. 4, 5

- [22] Jeong-gi Kwak, Erqun Dong, Yuhe Jin, Hanseok Ko, Shweta Mahajan, and Kwang Moo Yi. Vivid-1-to-3: Novel view synthesis with video diffusion models. *arXiv preprint arXiv:2312.01305*, 2023. 1, 2, 6, 7
- [23] Black Forest Labs. Flux. <https://github.com/black-forest-labs/flux>, 2024. 1
- [24] Visual Layer. imagenet-1k-vl-enriched. <https://huggingface.co/datasets/visual-layer/imagenet-1k-vl-enriched>, 2024. 4
- [25] Chendi Lin, Heshan Liu, Qunshu Lin, Zachary Bright, Shitao Tang, Yihui He, Minghao Liu, Ling Zhu, and Cindy Le. Objaverse++: Curated 3d object dataset with quality annotations, 2025. 4, 5
- [26] Hao Liu, Wilson Yan, Matei Zaharia, and Pieter Abbeel. World model on million-length video and language with ringattention. *arXiv preprint*, 2024. 1
- [27] Minghua Liu, Chao Xu, Haian Jin, Linghao Chen, Mukund Varma T, Zexiang Xu, and Hao Su. One-2-3-45: Any single image to 3d mesh in 45 seconds without per-shape optimization. *Advances in Neural Information Processing Systems*, 36:22226–22246, 2023. 1, 2
- [28] Ruoshi Liu, Rundi Wu, Basile Van Hoorick, Pavel Tokmakov, Sergey Zakharov, and Carl Vondrick. Zero-1-to-3: Zero-shot one image to 3d object. In *Proceedings of the IEEE/CVF international conference on computer vision*, pages 9298–9309, 2023. 1, 2, 6, 7
- [29] Tianqi Liu, Guangcong Wang, Shoukang Hu, Liao Shen, Xinyi Ye, Yuhang Zang, Zhiguo Cao, Wei Li, and Ziwei Liu. Mvsgaussian: Fast generalizable gaussian splatting reconstruction from multi-view stereo. In *European Conference on Computer Vision*, pages 37–53. Springer, 2024. 1
- [30] Yuan Liu, Cheng Lin, Zijiao Zeng, Xiaoxiao Long, Lingjie Liu, Taku Komura, and Wenping Wang. Syncdreamer: Generating multiview-consistent images from a single-view image. In *The Twelfth International Conference on Learning Representations*, 2024. 1, 2
- [31] Xiaoxiao Long, Yuan-Chen Guo, Cheng Lin, Yuan Liu, Zhiyang Dou, Lingjie Liu, Yuexin Ma, Song-Hai Zhang, Marc Habermann, Christian Theobalt, et al. Wonder3d: Single image to 3d using cross-domain diffusion. In *Proceedings of the IEEE/CVF conference on computer vision and pattern recognition*, pages 9970–9980, 2024. 1
- [32] Tiange Luo, Chris Rockwell, Honglak Lee, and Justin Johnson. Scalable 3d captioning with pretrained models. *Advances in Neural Information Processing Systems*, 36:75307–75337, 2023. 5
- [33] Tiange Luo, Justin Johnson, and Honglak Lee. View selection for 3d captioning via diffusion ranking. In *European Conference on Computer Vision*, pages 180–197. Springer, 2024. 5
- [34] Ben Mildenhall, Pratul P Srinivasan, Matthew Tancik, Jonathan T Barron, Ravi Ramamoorthi, and Ren Ng. Nerf: Representing scenes as neural radiance fields for view synthesis. *Communications of the ACM*, 65(1):99–106, 2021. 2
- [35] Shen Nie, Fengqi Zhu, Zebin You, Xiaolu Zhang, Jingyang Ou, Jun Hu, JUN ZHOU, Yankai Lin, Ji-Rong Wen, and Chongxuan Li. Large language diffusion models. In *ICLR 2025 Workshop on Deep Generative Model in Machine Learning: Theory, Principle and Efficacy*, 2025. 1, 2, 3
- [36] Dustin Podell, Zion English, Kyle Lacey, Andreas Blattmann, Tim Dockhorn, Jonas Müller, Joe Penna, and Robin Rombach. Sdxl: Improving latent diffusion models for high-resolution image synthesis. *arXiv preprint arXiv:2307.01952*, 2023. 1
- [37] Aditya Ramesh, Prafulla Dhariwal, Alex Nichol, Casey Chu, and Mark Chen. Hierarchical text-conditional image generation with CLIP latents. *CoRR*, abs/2204.06125, 2022. 1
- [38] Robin Rombach, Andreas Blattmann, Dominik Lorenz, Patrick Esser, and Björn Ommer. High-resolution image synthesis with latent diffusion models. In *CVPR*, pages 10684–10695, 2022. 1
- [39] Ruoxi Shi, Hansheng Chen, Zhuoyang Zhang, Minghua Liu, Chao Xu, Xinyue Wei, Linghao Chen, Chong Zeng, and Hao Su. Zero123++: a single image to consistent multi-view diffusion base model. *arXiv preprint arXiv:2310.15110*, 2023. 1, 2, 6, 7
- [40] Yichun Shi, Peng Wang, Jianglong Ye, Long Mai, Kejie Li, and Xiao Yang. MVDream: Multi-view diffusion for 3d generation. In *The Twelfth International Conference on Learning Representations*, 2024. 2
- [41] Peize Sun, Yi Jiang, Shoufa Chen, Shilong Zhang, Bingyue Peng, Ping Luo, and Zehuan Yuan. Autoregressive model beats diffusion: Llama for scalable image generation. *arXiv preprint arXiv:2406.06525*, 2024. 1
- [42] Jiaxiang Tang, Jiawei Ren, Hang Zhou, Ziwei Liu, and Gang Zeng. Dreamgaussian: Generative gaussian splatting for efficient 3d content creation. In *The Twelfth International Conference on Learning Representations*, 2024. 1, 2
- [43] Aaron van den Oord, Oriol Vinyals, and koray kavukcuoglu. Neural discrete representation learning. In *Advances in Neural Information Processing Systems*. Curran Associates, Inc., 2017. 3
- [44] Zhou Wang, A.C. Bovik, H.R. Sheikh, and E.P. Simoncelli. Image quality assessment: from error visibility to structural similarity. *IEEE Transactions on Image Processing*, 13(4):600–612, 2004. 5
- [45] Chengyue Wu, Xiaokang Chen, Zhiyu Wu, Yiyang Ma, Xingchao Liu, Zizheng Pan, Wen Liu, Zhenda Xie, Xingkai Yu, Chong Ruan, et al. Janus: Decoupling visual encoding for unified multimodal understanding and generation. *arXiv preprint arXiv:2410.13848*, 2024. 1
- [46] Jianfeng Xiang, Zelong Lv, Sicheng Xu, Yu Deng, Ruicheng Wang, Bowen Zhang, Dong Chen, Xin Tong, and Jiaolong Yang. Structured 3d latents for scalable and versatile 3d generation. *arXiv preprint arXiv:2412.01506*, 2024. 1, 2, 6, 7
- [47] Shitao Xiao, Yuezhe Wang, Junjie Zhou, Huaying Yuan, Xingrun Xing, Ruiran Yan, Chaofan Li, Shuting Wang, Tiejun Huang, and Zheng Liu. Omnigen: Unified image generation. In *Proceedings of the Computer Vision and Pattern Recognition Conference*, pages 13294–13304, 2025. 1
- [48] Enze Xie, Junsong Chen, Yuyang Zhao, Jincheng Yu, Ligeng Zhu, Chengyue Wu, Yujun Lin, Zhekai Zhang, Muyang Li, Junyu Chen, et al. Sana 1.5: Efficient scaling of training-time

- and inference-time compute in linear diffusion transformer. *arXiv preprint arXiv:2501.18427*, 2025. 8, 1
- [49] Jinheng Xie, Weijia Mao, Zechen Bai, David Junhao Zhang, Weihao Wang, Kevin Qinghong Lin, Yuchao Gu, Zhijie Chen, Zhenheng Yang, and Mike Zheng Shou. Show-o: One single transformer to unify multimodal understanding and generation, 2025. 8, 1
- [50] Yi Xin, Qi Qin, Siqi Luo, Kaiwen Zhu, Juncheng Yan, Yan Tai, Jiayi Lei, Yuewen Cao, Keqi Wang, Yibin Wang, Jinbin Bai, Qian Yu, Dengyang Jiang, Yuandong Pu, Haoxing Chen, Le Zhuo, Junjun He, Gen Luo, Tianbin Li, Ming Hu, Jin Ye, Shenglong Ye, Bo Zhang, Chang Xu, Wenhai Wang, Hongsheng Li, Guangtao Zhai, Tianfan Xue, Bin Fu, Xiaohong Liu, Yu Qiao, and Yihao Liu. Lumina-dimoo: An omni diffusion large language model for multi-modal generation and understanding, 2025. 3, 6
- [51] Jiale Xu, Weihao Cheng, Yiming Gao, Xintao Wang, Shenghua Gao, and Ying Shan. Instantmesh: Efficient 3d mesh generation from a single image with sparse-view large reconstruction models. *arXiv preprint arXiv:2404.07191*, 2024. 5
- [52] Ling Yang, Ye Tian, Bowen Li, Xinchun Zhang, Ke Shen, Yunhai Tong, and Mengdi Wang. Mmada: Multimodal large diffusion language models. *arXiv preprint arXiv:2505.15809*, 2025. 1, 8
- [53] Yifan Yang, Houwen Peng, Yifei Shen, Yuqing Yang, Han Hu, Lili Qiu, Hideki Koike, et al. Imagebrush: Learning visual in-context instructions for exemplar-based image manipulation. *Advances in Neural Information Processing Systems*, 36:48723–48743, 2023. 3
- [54] Zebin You, Shen Nie, Xiaolu Zhang, Jun Hu, Jun Zhou, Zhiwu Lu, Ji-Rong Wen, and Chongxuan Li. Llada-v: Large language diffusion models with visual instruction tuning, 2025. 1, 3
- [55] Lijun Yu, Jose Lezama, Nitesh Bharadwaj Gundavarapu, Luca Versari, Kihyuk Sohn, David Minnen, Yong Cheng, Agrim Gupta, Xiuye Gu, Alexander G Hauptmann, Boqing Gong, Ming-Hsuan Yang, Irfan Essa, David A Ross, and Lu Jiang. Language model beats diffusion - tokenizer is key to visual generation. In *The Twelfth International Conference on Learning Representations*, 2024. 1, 3
- [56] Richard Zhang, Phillip Isola, Alexei A Efros, Eli Shechtman, and Oliver Wang. The unreasonable effectiveness of deep features as a perceptual metric. In *Proceedings of the IEEE conference on computer vision and pattern recognition*, pages 586–595, 2018. 5
- [57] Xuying Zhang, Yupeng Zhou, Kai Wang, Yikai Wang, Zhen Li, Shaohui Jiao, Daquan Zhou, Qibin Hou, and Ming-Ming Cheng. Ar-1-to-3: Single image to consistent 3d object generation via next-view prediction. *arXiv preprint arXiv:2503.12929*, 2025. 6, 7, 1
- [58] Ziyang Zhou, Pinghui Wang, Zi Liang, Haitao Bai, and Ruofei Zhang. Cross-modal 3d representation with multi-view images and point clouds. In *Proceedings of the Computer Vision and Pattern Recognition Conference*, pages 3728–3739, 2025. 1
- [59] Xianwei Zhuang, Yuxin Xie, Yufan Deng, Liming Liang, Jinghan Ru, Yuguo Yin, and Yuexian Zou. Vargpt: Unified understanding and generation in a visual autoregressive multimodal large language model. *arXiv preprint arXiv:2501.12327*, 2025. 1

A. Additional Experimental Details

A.1. Baseline Setting

Most of the baselines we select—such as Zero-1-to-3 [28], Zero-1-to-3 XL [7, 28], ViVid-1-to-3 [22], Zero123++ [39], EpiDiff [19], AR-1-to-3 [57], TRELIS [46], and our own method ViewMask-1-to-3 are trained on data rendered with perspective projection. Among all these methods, only MV-Adapter [18] is trained using data rendered with orthographic projection.

A.2. Experimental Settings

We train ViewMask-1-to-3 using 24 H200 GPUs with a total batch size of 384 and a learning rate of 3×10^{-5} . A cosine learning rate scheduler is adopted, and training is performed under the Zero-2 optimization strategy. During inference, we set the sampling steps to 20.

A.3. Ground-Truth Rendering

For Zero123++ and AR-1-to-3, the ground-truth images are rendered from 3D assets using their default six viewpoint configuration. MV-Adapter, follows its original training protocol and renders four orthographic views consistent with its orthographic camera model. For the remaining baselines that support arbitrary multi-view rendering, we use the same viewpoint and camera parameters as ours to ensure fair comparison.

For models such as Zero123++ that by default generate images with a gray background, we render the corresponding ground-truth views using the same background color when reporting PSNR, SSIM, and LPIPS. Although some implementations offer background removal via rembg, this often removes thin or delicate parts of the object as well, which in turn compromises the reliability of the baseline’s quantitative results.

Table 4. **Evaluation on Image Generation Benchmarks (GenEval).** Our model achieves strong performance in unified models and is also comparable to methods among generation-only models.

Model	Architecture	Single Obj.	Two Obj.	Counting	Colors	Position	Color Attr.	Overall
<i>Generation-Only</i>								
SDv1.5 [38]	Diffusion	0.97	0.38	0.35	0.76	0.04	0.06	0.43
SDv2.1 [38]	Diffusion	0.98	0.51	0.44	0.85	0.07	0.17	0.50
DALL-E 2 [37]	-	0.94	0.66	0.49	0.77	0.10	0.19	0.52
DALL-E 3 [3]	-	0.96	<u>0.87</u>	0.47	0.83	0.43	0.45	0.67
LlamaGen [41]	AR	0.71	0.34	0.21	0.58	0.07	0.04	0.32
FLUX.1 [Dev] [23]	Diffusion	0.98	0.81	<u>0.74</u>	0.79	0.22	0.45	0.66
SDXL [36]	Diffusion	0.98	0.74	0.39	0.85	0.15	0.23	0.55
OmniGen [47]	Diffusion	0.98	0.84	0.66	0.74	0.40	0.43	0.68
SANA-1.5 [48]	Diffusion	0.99	0.85	0.77	0.87	0.34	0.54	0.72
<i>Unified Understanding & Generation</i>								
SEED-X [12]	AR	0.97	0.58	0.26	0.80	0.19	0.14	0.49
LWM [26]	AR	0.93	0.41	0.46	0.79	0.09	0.15	0.47
Janus [45]	AR	0.97	0.68	0.30	0.84	<u>0.46</u>	0.42	0.61
Show-o [49]	AR+Diff.	0.98	0.80	0.66	0.84	0.31	0.50	0.68
VAR-GPT [59]	AR	0.96	0.53	0.48	0.83	0.13	0.21	0.53
MMaDA [52]	Discrete Diff.	0.99	0.76	0.61	0.84	0.20	0.37	0.63
ViewMask-1-to-3	Discrete Diff.	0.99	0.88	0.50	<u>0.86</u>	0.60	<u>0.53</u>	0.72

B. Additional Results

B.1. Image to Multi-view Images

We provide additional I2MV comparison results, as shown in Fig. 8. Our model demonstrates more accurate control over fine-grained details.

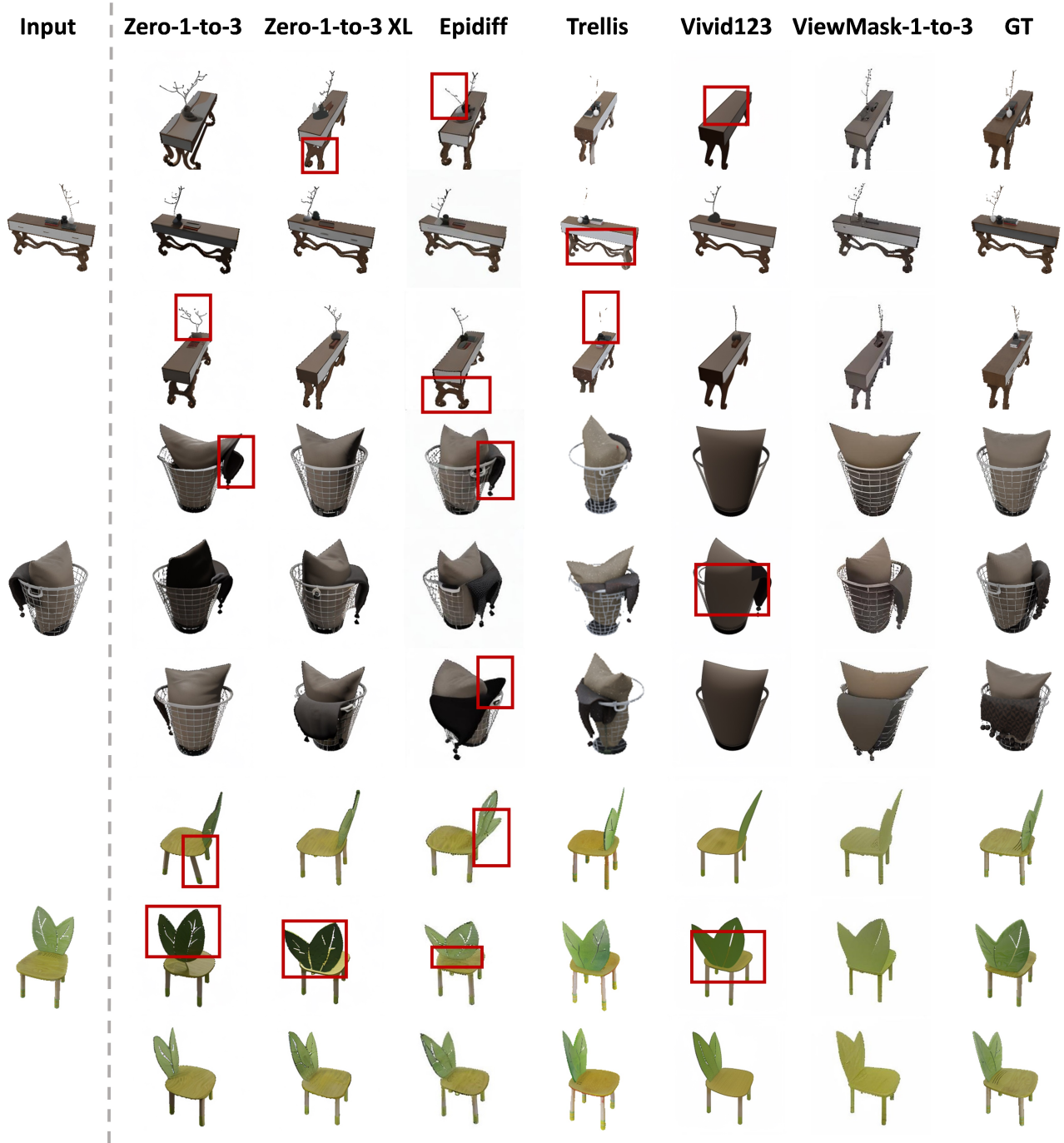


Figure 8. **Qualitative comparison on the 3D-Future dataset.** Visual results on the 3D-Future dataset, showing that our ViewMask-1-to-3 produces more consistent and realistic novel views compared with recent methods.

B.2. Task Extension

Unified Multimodal Understanding and Generation. During inference, ViewMask-1-to-3 employs task-specific input templates that leverage discrete tokens for both vision and language modalities. For multimodal understanding (MMU)

tasks, the input sequence is structured as:

$$[\text{MMU}] [\text{SOT}] \textit{prompt} [\text{EOT}] [\text{SOI}] \textit{image tokens} [\text{EOI}]$$
$$[\text{SOT}] \textit{answer} [\text{EOT}],$$

where the text prompt and visual content are presented sequentially to guide the model’s comprehension and response generation. The red-highlighted tokens correspond to the fully masked answer region, representing the content the model must produce.

For text-to-image (T2I) task, the sequence follows:

$$[\text{T2I}] [\text{SOT}] \textit{caption} [\text{EOT}] [\text{SOI}] \textit{image tokens} [\text{EOI}],$$

where the model autoregressively generates image tokens after the caption prompt.

We quantify the text-to-image generation capability of our model on GenEval, which evaluates object-centric generation under compositional prompts with diverse object attributes. Table 4 shows that ViewMask-1-to-3 achieves a strong overall score of 0.72, outperforming the architecturally similar MMaDA by 14% (0.72 vs. 0.63), highlighting the practical potential of discrete diffusion architectures.